(Proc. of JS.1 at the Joint IAHS & IAH Convention, Hyderabad, India, September 2009). IAHS Publ. 328, 2009.

Estimation of hydrological dynamics and ecohydrological effects in the Karst region of southwest China

XI CHEN, ZHICAI ZHANG, PEN SHI & XUANWU XUE

State Key Laboratory of Hydrology-Water Resources and Hydraulic Engineering, Hohai University, Nanjing 210098, China

xichen@hhu.edu.cn

Abstract Temporal and spatial distributions of hydrological processes are key drivers on Karst ecological systems through changing soil moisture dynamics, nutrient cycling and vegetation cover. This study investigates Karst basin hydrological processes through modelling of the interactions between hydrology, rock and soil, and vegetation. A distributed hydrological model was developed by integrating hydrological dynamics of porous and fissure flows. A small Karst basin, with detailed observation data of hydro-geological conditions and eco-hydrological processes, was selected for model calibration and validation. The results show that the new model is able to capture the sharp rise and decrease of the underground streamflow hydrograph. The simulated soil moisture content and evapotranspiration reveal impacts of epikarst and vegetation cover on hydrology.

Key words Karst; ecohydrology; vegetation; distributed ecohydrological model

INTRODUCTION

Karst terrain covers about 15% of the world's land area, or about 2.2 million km^2, and is home to around 1 billion people (17% of the world's population) (Yuan & Chai, 1988). About 25% of the world's population is supplied largely or entirely by Karst waters, including deep carbonate aquifers (Ford & Williams, 1989). China's Guizhou Province, located on the east side of the Yunnan-Guizhou Plateau, has one of the largest, continuous Karst areas in the world. It covers 1.76×10^6 km^2 and has a population of 32.4 million. About 73% of the land surface in Guizhou is Karst, which is underlain by up to 10 000 m of soluble carbonate rocks, 10% is hilly, and only 3% is classified as flat (Zeng, 1994). Mountainous areas with slopes of more than 15° account for 60% of its area (Li *et al.*, 2002). The region contains a full suite of Karst landforms, including poljes, cockpits, towers and dolines.

In the Karst region of south China, soils developed on carbonate rocks are generally 50 cm thick. This near-surface weathered zone of the exposed carbonates is called epikarst. Limestone fragments are mixed in soils and can act as a controlling factor for erosion rates and patterns in the landscape. Outcrop and embedded rock and its fractures, vegetation root and human actions, such as fire and forming, result in strong heterogeneity of soil composition and structures, and thus spatial patterns of soil moisture content (SMC) and hydraulic conductivity.

The simulations of the Karstic spring hydrographs were achieved by using two main modelling methods: (i) physical, or mathematical models, and (ii) lumped models, with two different approaches either as black- or grey-box or reservoirs. Mathematical, distributed models are usually based on numerical groundwater models, e.g. MODFLOW and Feflow, in the same way as for porous or fractured aquifers. They are improved to be able to represent the flow conditions in the saturated zone of Karst aquifers in an underground conduit-and-fracture network through a porous matrix. However, the groundwater-based models do not describe the spatial distribution of soil moisture, hillslope surface water and evapotranspiration from soil or epikarst. Therefore, this kind of model is not suitable for estimation of hydro–ecological relationships.

Distributed hydrological models, like TOPMODEL (Beven & Kirkby, 1979) and DHSVM (Wigmosta *et al.*, 1994), describe hydrological processes, especially surface, subsurface and groundwater flows. They are often used to evaluate the impact of climatic change and land use and cover (LULC) on hydrology and water resources because they are easily developed to integrate with climate model and ecological processes.

In this study, we improved on a distributed hydrology-soil-vegetation model (DHSVM) on the basis of integrated hydrological processes in the porous and fissured media of the Karst basin. In the improved DHSVM, a mixed runoff routing method integrating interactions among Darcy flow, fissure flow and channel storage routing, was developed. The improved model was applied in a small watershed of Chenqi within the Puding Karst Ecohydrological Observation Station, Guizhou province, China. The model was calibrated and validated based on the observation data of streamflow, vegetation interception and soil moisture contents. Modelling results reveal spatial distribution of hydrological processes influenced by the Karst basin LULC.

METHODS

DHSVM

The Distributed Hydrology-Soils-Vegetation Model (DHSVM) is a physically-based distributed parameter model that provides a DEM based representation of a watershed (Wigmosta *et al.*, 1994). The spatial scale of the representation is based on the grid size of the DEM. The model consists of a two-layer canopy (overstorey vegetation, understorey vegetation) representation of evapotranspiration, a two-layer energy balance model for ground snow pack, a multilayer unsaturated soil model, a saturated subsurface flow model, and a 3-D overland flow representation. The DEM provides the topographic controls on the incoming short-wave radiation, precipitation, air temperature, and downslope water movement. Grid cells are assigned vegetation and soil characteristics, and are hydrologically linked through surface and subsurface flow routing.

Karstic flow system and modelling methods

Soil and epikarst zones in the Karst basin are important for water storage and movement. The near-surface weathered zone of the exposed carbonates (epikarst) has a large permeability, offering a fast water infiltration. Water tends to accumulate at the base of a well developed epikarstic zone because the infiltration capacity at the surface is much greater than the rate of downwards percolation through the underlying transmission zone. It forms temporarily-stored water that constitutes the epikarstic aquifer. Some of the temporarily-stored water penetrates into the deep aquifer because not all fissures are closed tight at the base of the epikarst (Williams, 2008). Groundwater in the deep aquifer flows through interconnected, solutionally-enlarged conduits and cave systems, and eventually flows out of the basin as a spring.

The Karst basin is divided into three zones in a vertical direction: upper soil, epikarst and deep aquifer. A multi-layer model is used to account for soil moisture and subsurface flow dynamics:

$$d_1(\theta_1^{t+\Delta t} - \theta_1^t) = P_0 - P_1(\theta_1) - E_{to} - E_{tu} - E_s + V_{sat} - V_r \tag{1}$$

$$d_2(\theta_2^{t+\Delta t} - \theta_2^t) = P_1(\theta_1) - P_2(\theta_2) - E_{to} + V_{sat} \tag{2}$$

$$d_3(\theta_3^{t+\Delta t} - \theta_3^t) = P_2(\theta_2) - P_3(\theta_3) + (Q_{\sin}^t - Q_s^t)\Delta t \tag{3}$$

$$S^{t+\Delta t} - S^t = P_3(\theta_3) + (Q_{din}^t - Q_d^t)\Delta t \tag{4}$$

where d_1, d_2 are soil or/and epikarst thickness of the upper and lower rooting zones, respectively, d_3 is the left epikarst thickness, θ_n (n = 1, 2, 3) is the average soil moisture content of nth zones, P_0 is the volume of infiltrated rainfall, V_{sat} is the volume of water supplied by a rising water table, V_r is the volume of return flow (generated when a rising water table reaches the ground surface), E_{to} and E_{tu} are evapotranspiration from overstorey vegetation (o) and understorey vegetation (u), respectively, E_s is soil evaporation, $P_n(\theta)$ (n = 1,2,3) is downward volumes of water discharged from nth zones over the time step, $Q_{\sin}^t$ and Q_s^t are subsurface flow rate to pass in and out the epikarst zone, respectively, $S^{t+\Delta t}$ and S^t are groundwater storage of deep aquifer at time $t + \Delta t$ and t, respectively, Q_{din}^t and Q_d^t are groundwater flow rate to pass in and out the deep aquifer, respectively.

Unsaturated movement through multiple rooting zone soil layers, $P_n(\theta)$, is calculated using Darcy's law assuming a unit hydraulic gradient:

$$P_n(\theta) = K_v(\theta) \quad (5)$$

where $K_v(\theta)$ is the vertical unsaturated hydraulic conductivity. The Brooks-Corey (Brooks & Corey, 1964) equation is used to calculate hydraulic conductivity:

$$K_v(\theta) = K_v(\theta_s)[\frac{\theta - \theta_r}{\phi - \theta_r}]^{(2/m)+3} \quad (6)$$

where m is the pore size distribution index, ϕ is the soil porosity, and θ_r is the residual soil moisture content. For simplicity, the saturated moisture content θ_s is taken equal to ϕ.

The epikarstic zone primarily consists of a fractured medium. The mathematical formulation of the average velocity of groundwater flow in fractures is given by the "cubic law" (Kiraly, 1969; Snow, 1969). The transmissivity and hydraulic conductivity of fractured media can be expressed as follows:

$$T_{i,j} = mC\frac{\rho g b_{i,j}^3}{12\mu} \quad (7)$$

$$K_{i,j} = mC\frac{\rho g b_{i,j}^2}{12\mu} \quad (8)$$

where m is the fractural number, C is a coefficient which is related with the roughness of the fracture surfaces and fracture aperture, $b_{i,j}$ is the fracture aperture at grid i,j, μ is dynamic viscosity of water, ρ is fluid density, g is acceleration due to gravity.

Infiltration and percolation $P_n(\theta_n)$ in the epikarst zone is calculated by equations (5) and (6) with large vertical $K_v(\theta_s)$ estimated by equation (8).

For the upper two layers, soil and fractured rock are often interconnected. An equivalent hydraulic conductivity $K_v(\theta_s)$, can be used to compute infiltration and percolation in the upper two layers as follows:

$$Kv(\theta_s)_{i,j} = \frac{Kvs_{i,j}ds + Kvf_{i,j}df}{ds + df} \quad (9)$$

where $Kvs_{i,j}$ and $Kvf_{i,j}$ are vertical hydraulic conductivities for soil and epikarst, respectively, and ds and df are their thickness. Thus, $K_v(\theta_s)$ equals Kvf in the exposed base rock areas, and $K_v(\theta_s)$ equals Kvs in the deep soil areas.

In the saturated zone, subsurface water flows to the main spring through the conduit system, which collects the water stored: (i) in epikarstic aquifer, and (ii) in deep aquifer. Water flows from both aquifers are calculated by the following equation with different values of horizontal transmissivities.

$$q(t)_{i,j,k} = w_{i,j,k} f_{i,j,k} T(t)_{i,j} \quad (10)$$

where $w_{i,j,k}$ is the grid (i, j) width at k flow direction, $T(t)_{i,j}$ is hydraulic transmissivity for grid (i, j), $f_{i,j,k}$ is flow fraction for cell i,j in direction k.

Vertical variations of hydraulic conductivity and transmissivity in the epikarst zone depend on fracture aperture and spacing. Limestone fracture aperture may be as large as 1×10^{-2} m in the exposed surface, decreasing to $1 \times 10^{-3} - 1 \times 10^{-4}$ m in compact and impermeable bed rock. Because the fracture aperture and spacing exponentially decrease towards base of the epikarst, hydraulic conductivity is assumed to decrease exponentially with depth ($Ks = Ks_0e^{-\alpha z}$). Thus:

$$T(t)_{i,j} = \frac{Ks_{i,j}}{\alpha_{i,j}}(e^{-\alpha_{i,j}z_{i,j}} - e^{-\alpha_{i,j}D_{i,j}}) \quad (11)$$

where $Ks_{i,j}$ is the lateral component of saturated hydraulic conductivity for cell i, j at epikarst surface, $Z_{i,j}$ is the distance from the ground surface to the water table (positive downward), $\alpha_{i,j}$ is a parameter related to the decay of saturated conductivity with depth, and $D_{i,j}$ is the total epikarst depth.

For groundwater flow in the matrix and fracture of the deep aquifer, equation (11) can be adopted to calculate $T(t)_{i,j}$, in which $Ks_{i,j}$ is the lateral saturated hydraulic conductivity at epikarst base rock, and $Z_{i,j}$ is the distance from the epikarst base level to the groundwater table, and $D_{i,j}$ is the total groundwater aquifer depth from the epikarst base to the base lines of mature conduits. Epikarst porosity ranges between 1 (Smart & Friederich, 1986) and 2–10% (Gouisset, 1981) and 5–10% (Willliams, 1985). A larger porosity of 5–10% is selected for the epikarst zone and the smaller porosity of 1–5% for the deep aquifer.

In Karst basins, strong anisotropy of the Karst fracture may dominate subsurface flow directions in addition to topography. Thus, a formula was developed to calculate the flow fraction for cell *i,j* in direction *k*, denoted $f_{i,j,k}$, considering topographic slope or groundwater slope $\beta_{i,j,k}$ and aquifer anisotropy:

$$f_{i,j,k} = p_{i,j,k}\beta_{i,j,k} \tag{12}$$

where $p_{i,j,k}$ $\left(= \frac{T_{i,j,k}}{\sum_{k=1}^{8} T_{i,j,k}}\right)$ is a flow fraction for cell *i,j* in direction *k* resulting from Karst fractural anisotropy.

The conduit systems within aquifers often exhibit branch work patterns as small tributaries draining individual closed depressions merge to form larger drainage channels which ultimately lead to a spring (Fig. 1) (White, 1999). Dendritic paths are assumed to be similar to surface channel networks. Flow in the stream channels is routed using a series of cascading linear channel reaches. Individual hydraulic parameters describe each reach. As the reach passes through grid cells, lateral inflow into the channel reach consists of both overland flow and subsurface flow. Flow is routed between channel reaches as a linear routing algorithm where each reach is treated as a reservoir of constant width, with outflow linearly related to storage (refer to Wigmosta *et al*., 1994 in detail).

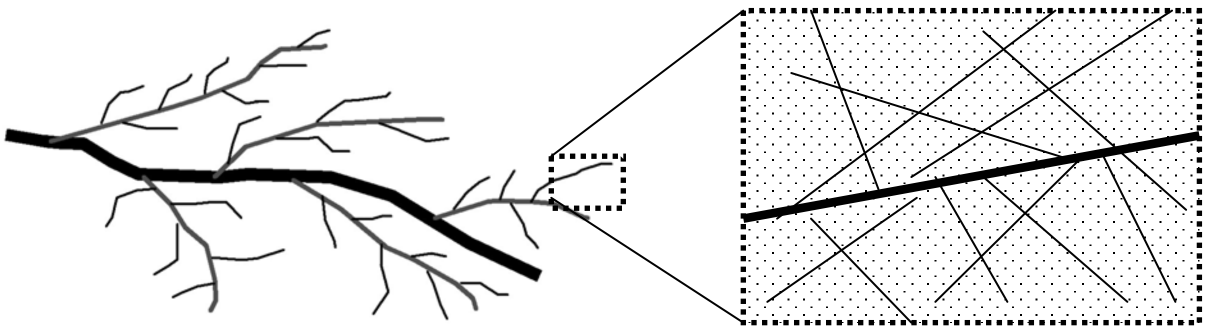

Fig. 1 Groundwater channel network.

APPLICATION

Study area and site description

The Chenqi catchment located in the Puding Basin, Guizhou Province, China has a catchment area of 1.5 km^2 (Fig. 2). The study site has a subtropical wet monsoon climate with a mean annual temperature of 20.1°C. The highest average monthly temperature is in July, and the lowest is in January. Annual precipitation is 1140 mm, with a distinct summer wet season and a winter dry season. Average monthly humidity ranges from 74% to 78%. The elevation of the study area above sea level varies from 1320 to 1520 m. With the typical cone Karst and cockpit Karst geomorphology of rugged terrain and steep slopes, the cone peaks of Chenqi catchment are generally 200 m above the adjacent doline depressions. Geological properties include dolostone, thick and thin limestone, marlite and Quaternary soil (Fig. 2).

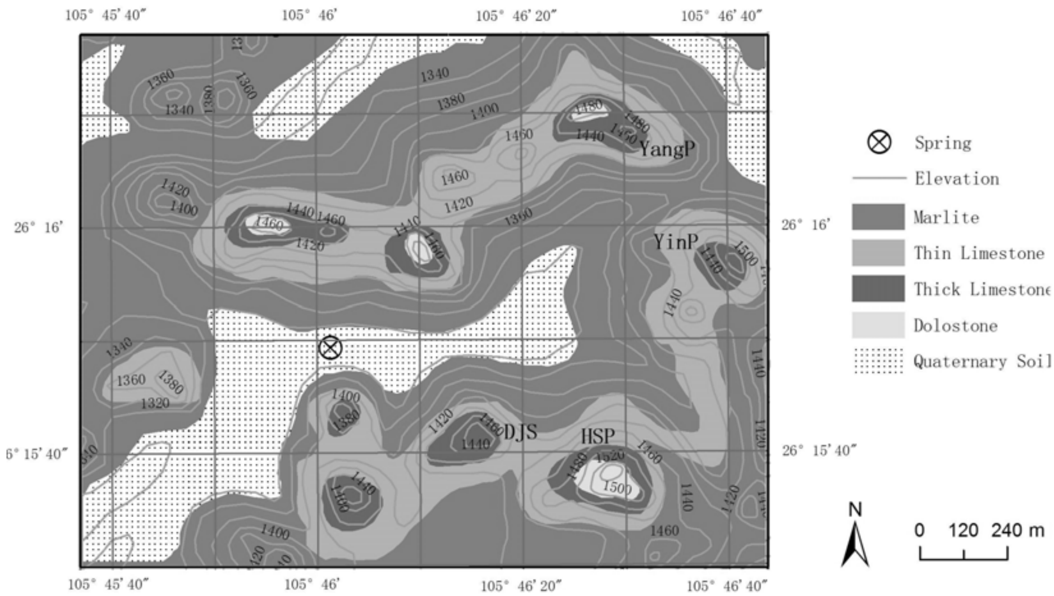

Fig. 2 Topography and geology in Chenqi basin.

The vegetation species include grasses, Karst montane deciduous broad-leaved shrubs and evergreens and deciduous broad-leaved mixed forest (Fig. 3). In the forest area, tree height varies from 2 to 5 m and its canopy fraction is about 80–90%; rock outcrop rate is 20–40%. In the shrub area, tree height varies from 1 to 1.5 m and its canopy fraction is 20–50%; rock outcrop rate is 30–50%. In the grass area, the canopy fraction is about 80%; rock outcrop rate is 35%. Parameters related to vegetation are determined on the basis of the field investigation and Land Data Assimilation System (LDAS) (http://ldas.gsfc.nasa.gov/LDAS8th/MAPPED.VEG/LDASmapveg.shtml).

Distribution of soil properties, e.g. soil types, composition and density, are determined through field investigation and laboratory experiments from 49 soil samples. Generally, soil can be divided into upper and lower layers with regard to different soil composition in the vertical direction. The soil of the upper 20 cm is classified into two types: silt loam in the low and depression areas and sandy loam in the middle and upper hill areas (Fig. 3). The bulk density ranges from 0.66 to 0.9 g/cm^3 and porosity from 0.2 to 0.4. The lower layer is primarily the brown clay with high calcium content. Its density is 1–1.28 g/cm^3 and porosity 0.42–0.48. The average soil thickness along the hillslopes with vegetative cover is <50 cm. Soil in the farm fields can reach 2 m in thickness due to earth moving by farmers. In the DHSVM, a soil class is assigned to each model pixel. Weighted averages of percent sand, silt, and clay were calculated for each soil class and layer. Most of the soil parameters that describe each soil class were obtained from laboratory analysis.

In situ experiments for determination of saturated hydraulic conductivity (K) were executed at 15 measuring points using a Guelph-Infiltrometer (GUELPH). The upper soil K varies from 0.18 m/day for silt loam, to as large as 12.7 m/day for sandy loam mixed with fractured rock. Lower layer soil is usually compact and K is less than 0.1 m/day.

Field investigations for fracture distribution were made at 22 sites in the study region. Mean fracture aperture is 0.0136 m, with mean squared error of 0.0157 m; mean fracture spacing is 0.142 m with mean squared error of 0.0986 m. Fracture aperture and spacing are randomly generated in light of a normal distribution function. Fracture aperture is assumed to decrease exponentially, from 0.0136 m on the ground surface to 0.001 m in compact and impermeable

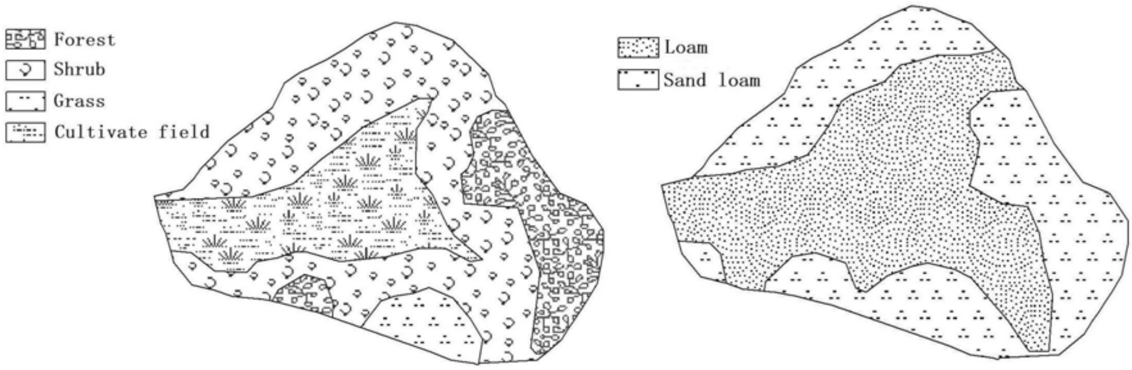

Fig. 3 Classification of vegetation and soil.

limestones. The weight *p* of fracture isotropy is randomly generated on the basis of uniform distribution of *p* value between 0 and 1 in the eight directions.

A set of meteorological and eco-hydrological observation stations was established from June 2007 in the Chenqi catchment. Three meteorological stations are located at DJS, HSP and YinP for observation of precipitation, air temperature and pressure, relative humidity, wind speed, and radiation, on a time interval of 5 minutes. Four groups of the soil moisture probes at depths of 15 and 30 cm below the ground surface were installed at DJS, YinPu, HSP and YanP, automatically recording soil moisture content every 5 minutes. Ten rainfall collection tubes with diameter of 29 cm under the forest area of DJS, were used to collect the penetrating amount of every rainfall event. An automatic water level observation station was installed at the catchment outlet to record water level at a 15-min time step.

The gridded DEM required by the model was derived from the 1:10 000 digital topography map from the Puding Karst Ecosystem Observation Station, Guizhou Province, China. The resulting rectangular subset 10 m × 10 m resolution DEM containing 16 950 pixels (113 rows by 150 columns) was analysed to delineate the basin boundary. The underground channel drainage network was initially derived from the DEM on the assumption that large underground channels are located in the lower basin areas. The channel network was further edited through field surveys. GIS analysis was used to determine the channel orders, and to assign mean values of channel width, depth, and Manning roughness for each order. Three orders of the underground channel network were generated, ranging 1–3 m for channel depths and 0.3–1.5 m for widths.

Model calibration and validation

Calibration of physically based distributed models such as the DHSVM requires particular attention because of the number of parameters involved (e.g. Beven, 1989). Equivalence of different parameter combinations (parameter equifinality) is usually expected, and this causes non-uniqueness of the model calibration. The problem of parameter equifinality can, to some extent, be overcome by considering different hydrological processes that can be separated using the calibration data (soil moisture, rainfall interception, flow routing) in a sequential fashion during model calibration. The calibration approach was taken as following: (1) model parameters affecting rainfall interception were optimized using the measured data at YanP (Fig. 4); (2) parameters affecting soil moisture contents were optimized making use of SMC data measured at the four sites (Fig. 5); (3) parameters affecting runoff generation from epikarst zone and groundwater aquifer were constrained using the basin outflow hydrograph of flood events and baseflow, respectively (Figs 6 and 7). In each calibration step, the four large flood discharges from 28 July 2007 to 19 October 2007 were used for the model initiation and calibration, and the period from 20 April 2008 to 26 June 2008 was held back for the verification. The computation step is 1 hour.

Eight rainfall events are selected to calibrate parameters of coefficients of canopy interception r_j, for overstorey vegetation (*o*) and understorey vegetation (*u*), respectively. Figure 4 shows that

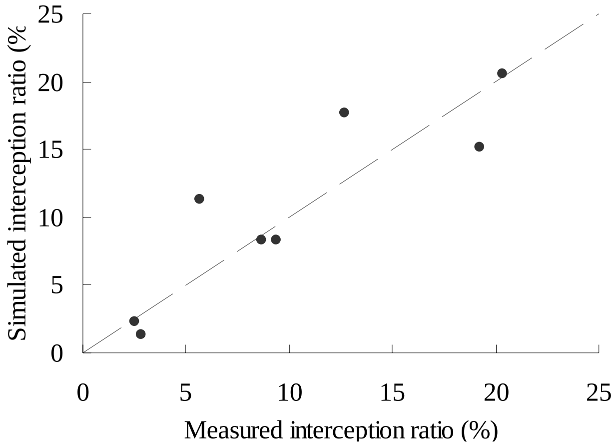

Fig. 4 Simulated and measured interception rate of vegetation.

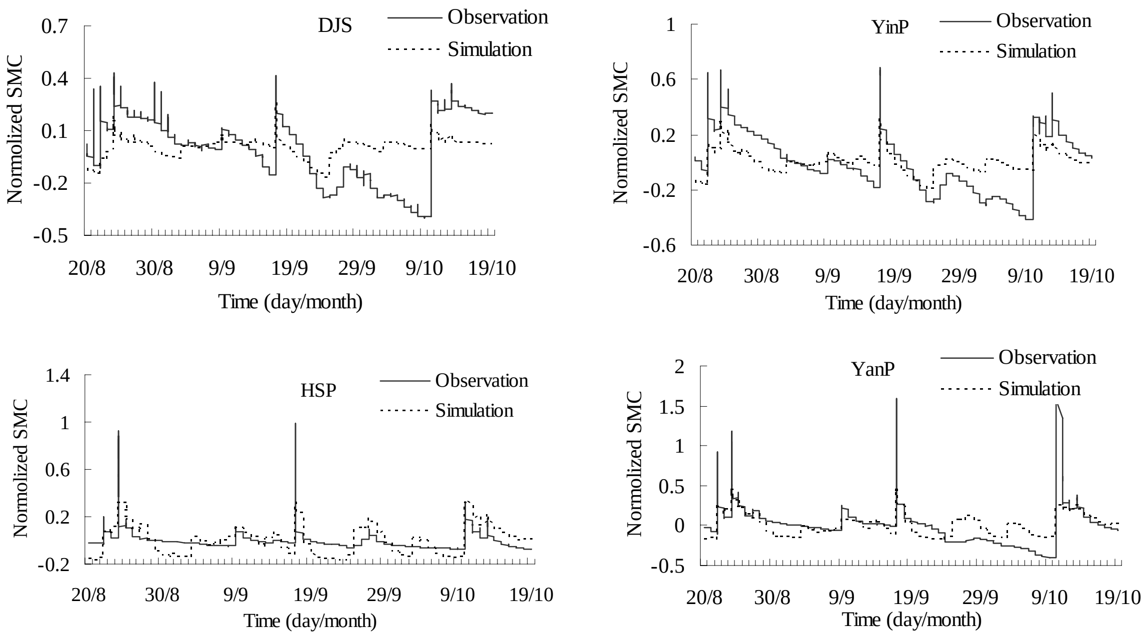

Fig. 5 Observed and simulated results of standardized SMC.

model calculated interception of forest matches well with observed values. Rate of interception by forest ranges between 3 and 25% for rainfall events with totals of 6.4–90.4 mm.

Two parameters of vertical saturated hydraulic conductivities for the upper soil and lower epikarst strongly influence infiltration, percolation and thus soil moisture contents. Simulated and observed SMCs at DJS, YinP, YanP and HSP have similar change patterns, represented by the normalized SMC. But magnitude of simulated and observed SMCs is different because simulated and observed SMCs represent average values within a grid of 10 × 10 m, and point values of the sensor, respectively.

For underground flow discharge simulation, three objective functions are selected for evaluating the success of the calibration: the relative volume error R_{ve} between the observed and simulated flows, the root mean squared error RMSE, relating how well the calculated and observed hydrographs compare in both volume and shape, and the coefficient of determination D, relating how well the calculated hydrograph compares in shape to that observed and depends only on timing, not on volume.

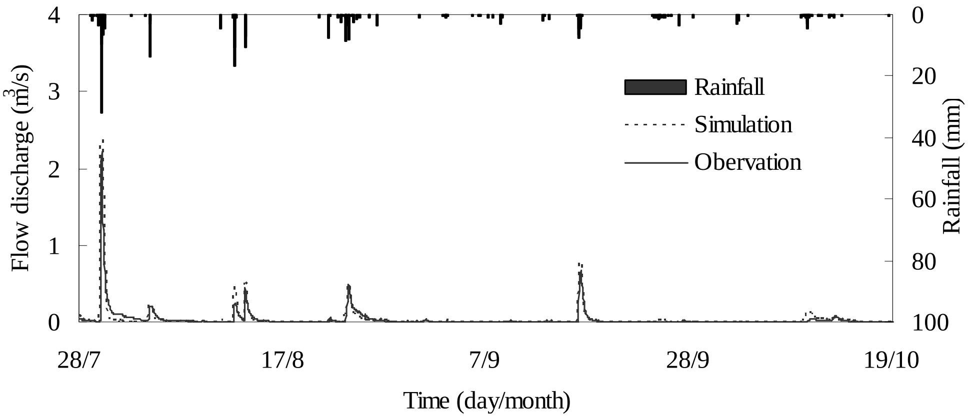

Fig. 6 Observed and simulated streamflow for model calibration.

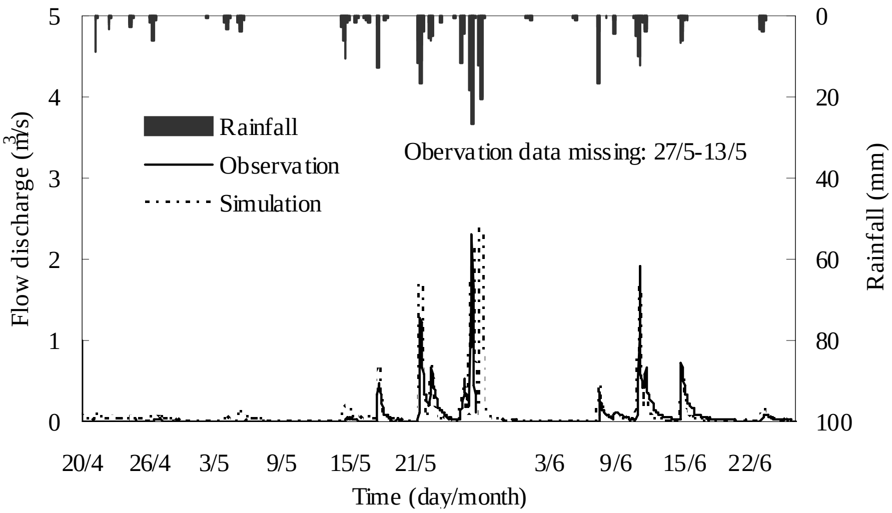

Fig. 7 Observed and simulated streamflow for model validation.

The model computation results were: R_{ve} = –0.018, RMSE = 0.05m^3/s, and D = 0.847 for the calibration period from 28 July 2007 to 19 October 2007; R_{ve} = 0.077, RMSE = 0.01 m^3/s, and D = 0.836 for the validation period from 20 April 2008 to 26 June 2008. These results illustrate that adjustments to the lateral hydraulic conductivity profile suffice to match the outflow hydrograph with reasonable accuracy (Figs 6 and 7).

Epikarst and vegetation cover effects on hydrological processes

Model simulation results show that fractural density controls the flood volume through influencing infiltrated rainfall division between unsaturated and saturated zones. High density of fractures results in large infiltration and a sharp hydrograph, and thus little infiltrated water remains in soil and is lost through evapotranspiration. An example is shown in Fig. 8 with observed streamflow and simulated streamflows for scenarios where an epikarst zone exists (with epikarst influence) or is replaced with upper layer soil (without epikarst influence) during 29–31 July 2007. It shows that the epikarst zone significantly enhances flow response to rainfall events. Basin average SMC of the upper and lower layers of root zone overlying the epikarst is 0.135 and 0.368, respectively, and less than 0.158 and 0.39 when the epikarst zone is replaced with soil. Consequently, basin actual evapotranspiration increases from 0.047 to 0.07 mm/h.

Spatial distribution of soil moisture content (SMC) and actual evapotranspiration (ET) reveals integrated influences of topography, soil and Karst fracture, and land cover on hydrology. Figure 9

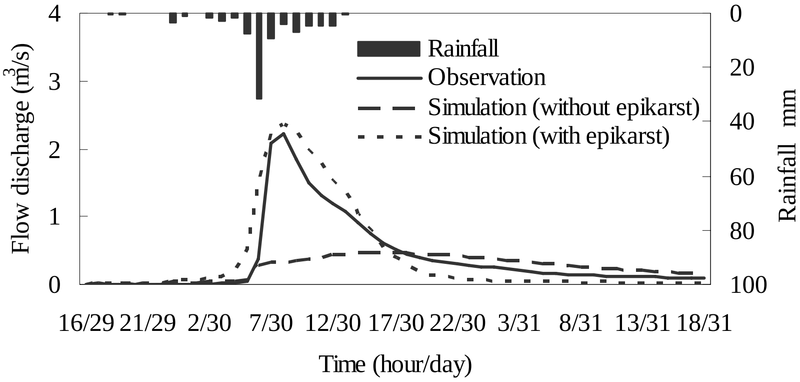

Fig. 8 Comparison of observed and simulated streamflow with and without epikarst.

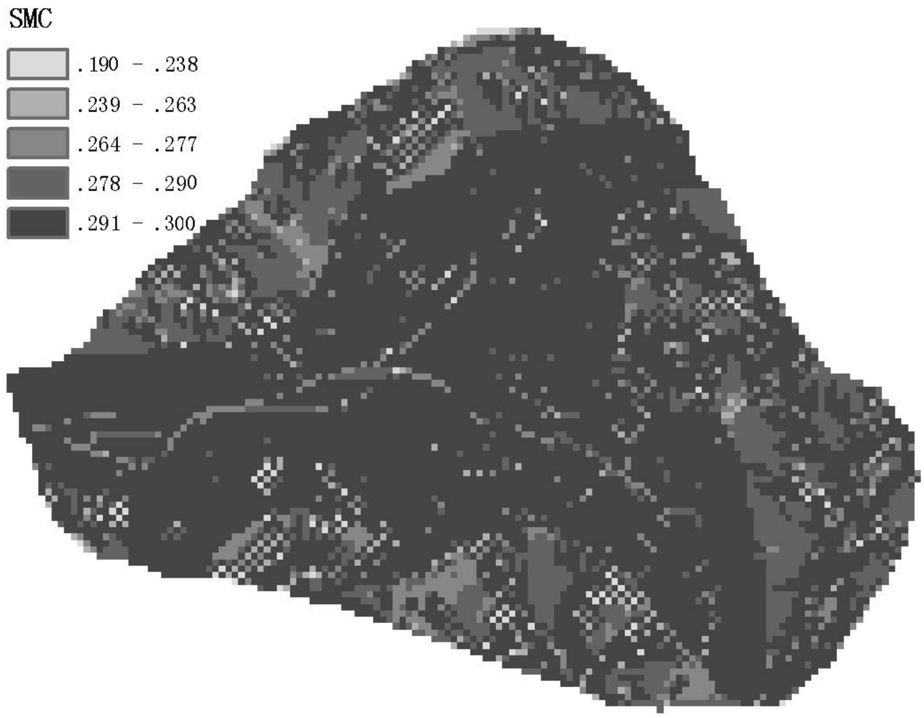

Fig. 9 SMC after a heavy rainfall.

shows that just after a heavy rainfall of 90.4 mm/day, SMC at 12 pm, 30 July 2007 primarily depends on topography, e.g. water concentration into low areas. Basin average SMCs for different land covers demonstrate that SMC at the upper soil layer is larger in the lower area of agricultural land than in the hillslopes with forest and shrub covers. However, SMCs are dominated by land covers due to evapotranspiration after a period of 6 consecutive non-rainfall days (12 pm, 11 August 2007). Statistical results from Fig. 10 demonstrate that forest ET at 12 pm is 0.053 mm, much larger than 0.016 and 0.012 mm in the shrub and bare soil areas, respectively. Figure 11 shows that SMC loss due to ET is primarily from the deep layer soil for forest, compared with those from the shallow layer in the shrub and bare soil areas. The upper layer soil in the forest cover areas has larger SMC than the shrub and agricultural areas (0.15 for forest *vs* 0.065 and 0.05 for shrub and agricultural areas, respectively). In the lower layer, SMC in the forest cover areas is 0.32, less than 0.37 and 0.34 in the shrub and agricultural areas, respectively. Spatial variation of the lower layer SMC is much less than those of the upper layer, indicating that climate change has a bigger influence on the upper soil than on the lower soil.

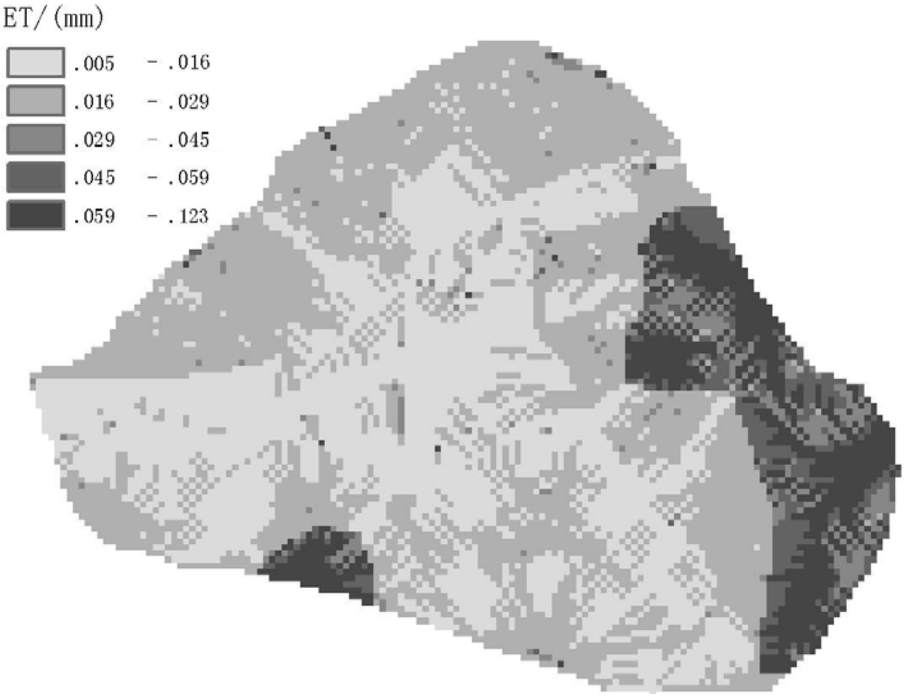

Fig. 10 ET after consecutive no-rainfall days.

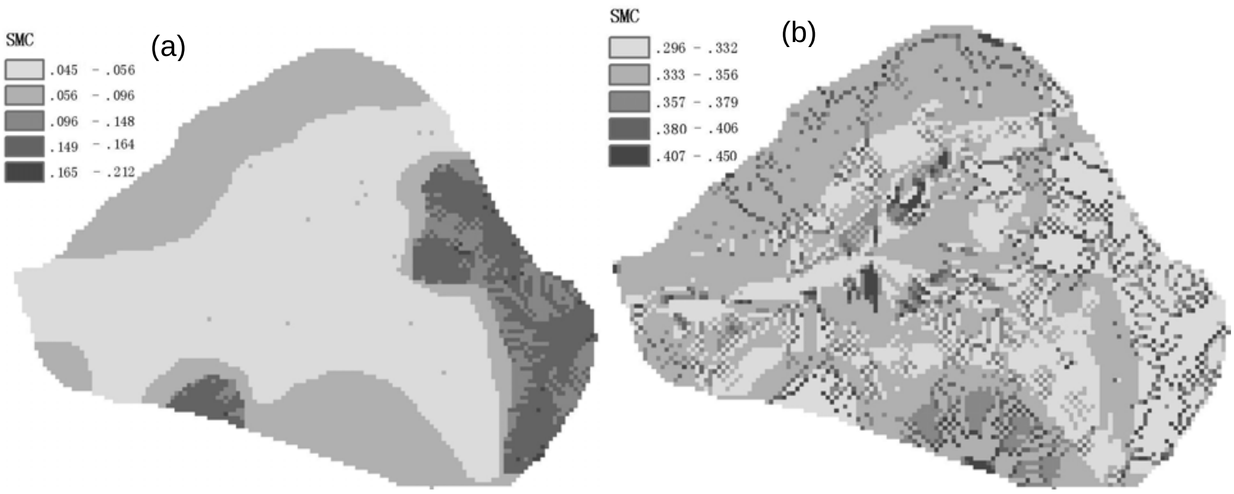

Fig. 11 SMC for the upper soil (a) and the lower soil (b).

CONCLUSIONS

Hydrology in the Karst basin is closely related to basin characteristics of fissured media in addition to topography, soil and vegetation. Modelling of water flow in the Karst basin should be based on runoff routing integrating Darcy flow, fissure flow and channel storage routing. In this study, a distributed hydrological model focused on epikarst fracture hydrological dynamics is developed on the basis of the Distributed Hydrology-Soil-Vegetation Model (DHSVM). The improved model was applied in a small watershed of Chenqi within the Puding Karst Ecohydrological Observation Station, Guizhou province of China. The model was calibrated and validated against the observation data of streamflow, vegetation interception and soil moisture. The results show that this improved model successfully captures the sharp rise and decrease of the streamflow hydrograph. It can also simulate soil moisture content and evapotranspiration associated with precipitation, Karst fracture and vegetation cover. This study is very useful for analysing ecohydrological processes and ecological and environmental effects under land cover and land use changes.

Acknowledgements This research was supported by National Basic Research Program of China (973 Program) (no. 2006CB403200), the Key Project of Chinese Ministry of Education (no. 308012), National Natural Scientific Foundation of China (no. 50679025), Programme of Introducing Talents of Discipline to Universities (no. B08048) and Program for Changjiang Scholars and Innovative Research Team in University, China. We are very grateful to Professors S. Wang and X. Bao for providing the observation data and collaboration in the research work.

REFERENCES

Beven, K .J. & Kirkby, M. J. (1979) A physically based variable contributing area model of basin hydrology. *Hydrol. Sci. Bull.* **24**(1), 43–69.

Beven, K. J. (1989) Changing ideas in hydrology – the case of physically based models. *J. Hydrol.* **105**, 157–172.

Ford, D. & Williams, P. (1989) *Karst Geomorphology and Hydrology*. Unwin Hyman, London, UK.

Gouisset, Y. (1981) Le Karst superficiel: genèse, hydrodynamique et caractéristiques hydrauliques, Univ. des Sciences et techniques du Languedoc, Montpellier, France, p. 218.

Király, L. (1969) Anisotropie et hétérogénéité de las perméabilité dans les calcaires fissurés. *Ecologae Geologica Helvetiae* **62**(28), 613–619.

Li, R., Wang, S. & Zhang, D. (2002) The role of man-made factors in ecoenvironmental detection in Guizhou Karst areas. *Bull. Mineralogy, Petrology & Geochemistry* **21**(1), 43–47.

Smart, P. L. & Friederich, H. (1986) Water movement and storage in the unsaturated zone of a maturely Karstified carbonate aquifer, Mendip Hills, England. In: *Proc. Conf. on Environmental Problems of Karst Terrains and their Solutions*, 59–87. (D. National Water Well Association, Ohio).

Snow, D. T. (1969) Anisotropic permeability of fractured media. *Water Resour. Res.* **5**(6), 1273–1289.

White, W. B. (1999) Groundwater flow and transport in Karst. In: *The Handbook of Groundwater Engineering* (ed. by J. W. Delleur). CRC Press LLC, USA.

Wigmosta, M. S., Vail, L. W. & Lettenmaier, D. P. (1994) A distributed hydrology-vegetation model for complex terrain. *Water Resour. Res.* **30**(6), 1665–1679.

Williams, P. W. (1985) Subcutaneous hydrology and the development of doline and cockpit Karst. *Zeitschriftfür Geomorphologie NF* **29**, 463–482.

Williams, P. W. (2008) The role of the epikarst in Karst and cave hydrogeology: a review. *Int. J. Speleology* **37**(1), 1–10.

Yuan, D. & Chai, G. (1988) *The Science of Karst Environment*. Chongqing Press, Chongqing, China.

Zeng, Z. (1994) Suggestion on poverty-deviation in the Karst mountain areas in south China. In: *Human Activity and Karst Environment* (ed. by Y. Xie & M. Yang), 15–19. Beijing Science and Technology Press, Beijing, China.